EurJIC
European Journal of Inorganic Chemistry

A Journal of ChemPubSoc Europe

Accepted Article

Title: Development of Efficient Copper-Based MOF-Derived Catalysts for the Reduction of Aromatic Nitro Compounds

Authors: Özlem Karahan, Emre Biçer, Adnan Taşdemir, Alp Yürüm, and Selmiye Alkan Gürsel

To be cited as: *Eur. J. Inorg. Chem.* 10.1002/ejic.201701320

Link to VoR: http://dx.doi.org/10.1002/ejic.201701320

WILEY-VCH

WILEY-VCH

FULL PAPER

Development of Efficient Copper-Based MOF-Derived Catalysts for the Reduction of Aromatic Nitro Compounds

Özlem Karahan [a]*, Emre Biçer [a], Adnan Taşdemir [b], Alp Yürüm [a], Selmiye Alkan Gürsel [a, b]

[a] *Sabancı University Nanotechnology Research and Application Center, 34956, Tuzla, İstanbul, Turkey*

[b] *Sabancı University Faculty of Engineering and Natural Sciences, 34956, Tuzla, İstanbul, Turkey*

Abstract: Two Copper-based $Cu_3(btc)_2$ and $Cu(Im)_2$ metal-organic frameworks were synthesized and annealed to form nanoporous Cu/Cu_2O@C and Cu@N-C nanoparticles for utilization as catalysts in the reduction reaction of aromatic nitro compounds to aromatic amines. All synthesized MOF compounds and MOF-derived nanoparticles were characterized using XRD, Raman, TGA, SEM-EDX and XPS methods. Also, the pore size distribution and surface area of the MOF-derived Cu/Cu_2O@C and Cu@N-C nanoparticles were characterized by BJH and BET methods. After characterization, the catalysts Cu/Cu_2O@C and Cu@N-C were catalytically tested for the reduction reactions of various aromatic nitro compounds chemically by monitoring via a UV-vis spectrometer. Both catalysts exhibited remarkable results compared with those in the literature. Also, the Cu/Cu_2O@C catalyst showed better results than the Cu@N-C catalyst.

Introduction

Metal-organic frameworks (MOFs) have attracted a great attention for two decades in various applications including adsorption [1], electrocatalyst [2] supercapacitors [3], batteries [4] and fuel cells [5]. Simply, MOFs consist of clusters containing a metal coordinated by rigid organic molecules to form two-dimensional and three-dimensional structures [6]. They possess high porosity, high specific surface area, low density and chemically-tunable structures [7]. Since MOFs present a large variety of tunable chemical features, they can be used instead of porous inorganic catalysts such as zeolites.

[a] Sabancı University Nanotechnology Research and Application Center 34956 Tuzla, İstanbul, Turkey.
ozlemkarahan@sabanciuniv.edu
http://sunum.sabanciuniv.edu

[b] Sabancı University Faculty of Engineering and Natural Sciences 34956 Tuzla, İstanbul, Turkey.

Supporting information for this article is given via

Recently there has been a wide interest in MOF-derived porous heterogeneous catalysts by the carbonization of organic linkers in MOF structure [8]. This approach not only increases internal surface area but also presents a larger pore size enabling catalytic reactions with catalyst metal on substrates and a stable metal-carbon hetero-structure in prolonged cycles when utilizing as a catalyst. Lin *et al.* has utilized a MOF-derived heterogeneous catalyst for the activation of oxone to decolorize of Rhodamine B in water by forming sulfate anion-radical [9]. Another approach for the use of MOF-derived compounds is to utilize them as an oxygen reduction reaction electrocatalyst for fuel cells and metal-air batteries. The usage of MOF-derived compounds provide a high specific surface area thus presents an excellent ORR activity [10]. In this regard, an interesting study on the salt-removal capacity of MOF-derived compounds was reported by Zhang *et al.* By using ZIF-8, a highly porous MOF together with cetyltrimethylammonium bromide (CTAB) to provide a highly porous structure hereby shows a great salt-adsorption capacity [11]. Zhang *et al.*, on the other hand, reported both NO reduction and DeNOx studies with excellent results by using MOF-derived Mn-based bimetallic MnO_x-FeO_y [12] and $Mn_xCo_{3-x}O_4$ [13] nanocages respectively. Moreover, the MOF-derived catalysts can be readily-synthesized, they are inexpensive and highly efficient compared with the inorganic-based equivalent counterparts.

The reduction of aromatic nitro compounds to aromatic amines is an important process since the products of the reaction have an industrial value as the intermediate precursors for the synthesis of pharmaceuticals, dyes, agrochemicals, antioxidants and corrosion inhibitors. Among them, 4-nitroaniline (4-NA) is the main precursor for the preparation of 1,4-phenylenediamine (PPD). However, the reduction reaction of aromatic nitro-group proceeds in two steps until complete reduction to aromatic amine compound. Two intermediate products, hydroxylamines and hydrazine, might be obtained as the side-products if the reaction is not truly completed [14, 15].

A noble metal assisted reduction have been demonstrated involving Pd, Pt, Ag and Au catalysts [16] with the use of H_2 gas as the co-catalyst. Nevertheless, the necessity of high H_2 gas pressures reduces recyclability and high temperatures present some limitations. On the other hand, other methods have been applied to reduce 4-NA to PPD. Wu *et al.* have proposed to reduce 4-NA in water under sunlight irradiation by a photocatalytic method with a CdS catalyst [17]. Similarly, the utilization of nanocrystalline $PbBi_2Nb_2O_9$ [18] and $SrBi_2Nb_2O_9$ [19] photocatalysts for the reduction of 4-NP to PPD are also reported. Another reduction technique was applied by Rathore *et al.* who reported that a core-shell iron oxide@nickel nanoparticles have successfully reduced aromatic nitro compounds to aromatic amino molecules with yields of 85-96% [16]. A sonochemical method was applied utilizing Fe_3O_4/SiO_2/Ag nanocubes by Abbas *et al.* and they reported that superior catalytic activity with 88% yields up to 15 reuse cycles [20]. Despite the promising results previously reported, complicated synthesis processes and prolonged reaction times are the main disadvantages in the studies mentioned above. On the other hand, there are other examples of MOF-derived catalysts efficiently proceeding a reduction reaction with the substrate of 4-nitrophenol [8, 21].

The catalytic effect of copper is extensively studied in the literature. Copper catalyzed C-H functionalization reactions [22], C-C bond cleavage reactions, reduction, oxidation and coupling reactions have been reported with copper-based compounds such as copper triflate, copper acetate, copper(I) iodide, copper (II) chloride, and copper (I) oxide [23]. However, a series of copper-based MOF compounds were utilized as catalyst in cyanosilylation reaction [24], isomerization of terpene derivatives [25], Biginelli reactions [26], Henry reactions [27], Click reactions [28], and epoxidation of olefins [29]. For instance, Schejn *et al.* used copper(II) as a dopant in ZIF-8 crystals demonstrating an excellent catalytic activity on [3+2] cycloadditions of organic azides to alkyne compounds. Moreover, the catalyst Cu/ZIF-8 has catalyzed both Friedlander and Combes reactions in high yields [30]. On the other hand, Wee *et al.* demonstrated an esterification reaction with acetic acid and 1-propanol catalyzed by $Cu_3(btc)_2$ nanocrystals encapsulated with phosphotungstic acid hydrate [31].

In the present study, we aimed to reduce aromatic nitro compounds using a facile, cost-effective and easily synthesized copper based MOF-derived catalysts with high porosity and high specific active surface area. For this reason, we synthesized $Cu_3(btc)_2$ and $Cu(Im)_2$ MOFs and then annealed the materials at an appropriate temperature for the first time to obtain copper-based composites to utilize them as a catalyst for the reduction of aromatic nitro compounds. A series of characterization have been utilized to identify the structure such as XRD, Raman, FE-SEM, TGA and XPS. The catalytic reduction reaction has been carried out in a quartz tube in the presence of the substrate, catalyst and co-catalyst $NaBH_4$. The reaction progress has been monitored with the formation of characteristic absorbance peak of aromatic amines and the disappearance of aromatic nitro absorbance peaks via UV-vis spectrometer. Consequently, remarkable kinetic results were obtained from the reduction of aromatic nitro compounds.

Results and Discussion

Characterization of MOF Compounds

The crystallinity of the synthesized $Cu_3(btc)_2$ compound was investigated using XRD analysis as depicted in Figure 1. As seen from the XRD pattern, the peaks at 6.5°, 9.5° and 12° were attributed to (200), (220) and (222) crystal planes of face-centered cubic (fcc) copper crystal structure, respectively. The XRD patterns of synthesized $Cu_3(btc)_2$ are in good agreement with the literature stating a successful synthesis of the $Cu_3(btc)_2$ MOF. The $Cu(Im)_2$ peaks are also confirmed according to literature by Luz *et al.* and Masciocchi *et al.* As shown in Figure 1, the XRD pattern of $Cu(Im)_2$ has the 7°, 11°, 13°, 17°, 20° and 34° peaks which are comparable with those reported in the literature [32, 33].

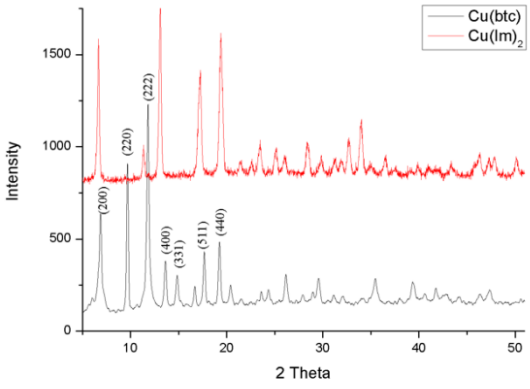

Figure 1. XRD patterns of $Cu_3(btc)_2$ and $Cu(Im)_2$

Raman spectrum for both $Cu_3(btc)_2$ and $Cu(Im)_2$ are illustrated in Figure 2. Seven bands are present at 225, 500, 745, 823, 1000, 1462 and 1605 cm^{-1} for the $Cu_3(btc)_2$, which are also in agreement with the literature [34] and are explained as follows: the band at 1605 cm^{-1} corresponds to the vibration stretching of benzene; the bands at 745 and 823 cm^{-1} can be out of plane ring (C-H) bending vibrations; the band at 1000 cm^{-1} is related to C=C bonds of the benzene ring; the band at 1462 cm^{-1} corresponds to the stretching of carboxylate groups; and the bands at 225 and 500 cm^{-1} can be attributed to vibrations of copper ions [35]. For the Raman spectrum of $Cu(Im)_2$, the bands at 950, 1147, 1150, 1290, 1495 and 1500 cm^{-1} are attributed to imidazole peaks [32].

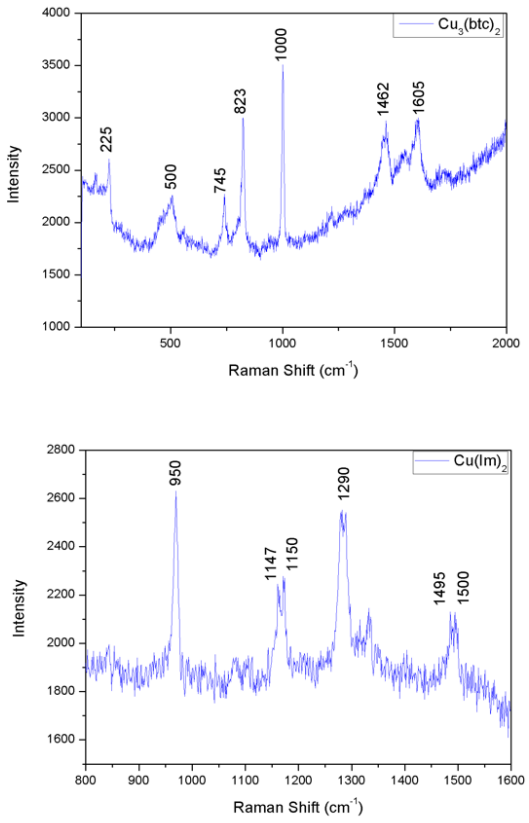

Figure 2. Raman data of $Cu_3(btc)_2$ and $Cu(Im)_2$

Thermal properties of the synthesized $Cu_3(btc)_2$ were investigated by using TGA under N_2-flow, as shown in Figure S7. It can be clearly seen that the $Cu_3(btc)_2$ molecule is stable up to 250°C and starts to decompose in the temperature range between 100°C and 200°C, indicating a hydrate release (10%) which is bonded or unbonded in the pores of the surface. A significant loss (47%) was observed between the temperature ranges of 270°C to 360°C, showing that the organic linkers of the MOF start to collapse to form Cu/Cu_2O@C composites. Upon this graph, a thermolysis temperature of 450°C was applied to synthesize a MOF-derived Cu/Cu_2O@C catalyst. Similarly, according to the TGA analysis of $Cu(Im)_2$, it starts to decompose at 270°C with a weight loss of 11%. In the temperature ranges between 360°C and 630°C, the main weight loss occurs by 43%, which is related to the collapse of organic linker groups. Thus, accordingly, the second MOF compound $Cu(Im)_2$ was thermolized at 650°C to obtain a Cu@N-C catalyst.

FE-SEM images of the MOF compounds $Cu_3(btc)_2$ and $Cu(Im)_2$ are shown in Figure 3. According to the SEM image of $Cu_3(btc)_2$, a top-cut rhombic octahedral morphology can be observed. Also, at high magnification, nano fibril formations were obtained. Thus, this structure increased the porosity of the material. On the other hand, $Cu(Im)_2$ resembles scattered needles.

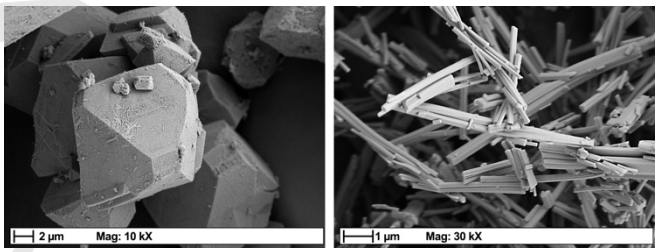

Figure 3. FE-SEM micrographs of $Cu_3(btc)_2$ (left) and $Cu(Im)_2$ (right)

Characterization of the Composites Cu/Cu_2O@C and Cu@N-C

The characterizations of Cu/Cu_2O@C and Cu@N-C composites were performed by using an XRD analysis. As seen in Figure 4, after the thermolysis of $Cu_3(btc)_2$ in an Ar atmosphere, two crystal phases were observed. One phase having peaks at 43°, 51° and 74° 2θ values are the (111), (200) and (220) crystal planes of Cu nanoparticles, respectively (JCPDS card no. 85-1326). Also, the rest of the peaks at 29°, 37°, 42° and 61° two-theta values were attributed to (110), (111), (200) and (220) crystal planes of Cu_2O nanoparticles, respectively (JCPDS card no. 78-2076) [36]. On the contrary, it is clearly seen that the thermolysis of $Cu(Im)_2$ yielded peaks at 42°, 51° and 74° 2θ values obtaining only a single Cu@N-C composite.

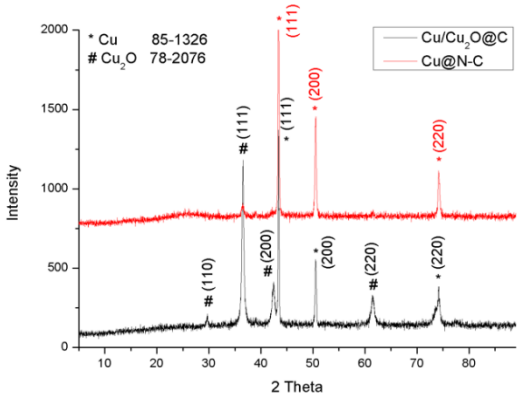

Figure 4. XRD analysis of $Cu_3(btc)_2$ thermolized at 450°C and $Cu(Im)_2$ thermolized at 650°C

After the thermolysis, the morphology of the MOF samples is shown in Figure 5. It can be seen that thermolized $Cu_3(btc)_2$ was transformed to a sponge-like structure and preserved its bipyramidal morphology. However, in the case of thermolized $Cu(Im)_2$, the needle-like structure completely disappeared, obtaining a somewhat flat morphology. Based on these results, it is possible to say that the thermolization of $Cu_3(btc)_2$ caused a highly porous morphology. Hence, its catalytic activity appears to be better than that of the thermolization of $Cu(Im)_2$.

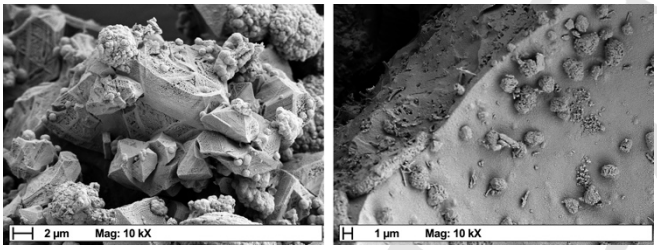

Figure 5. FE-SEM micrographs of the catalysts $Cu/Cu_2O@C$ (left) and Cu@N-C (right)

XPS spectra of the catalysts are given in Figure 6. As expected, after the thermolysis, $Cu_3(btc)_2$ derived $Cu/Cu_2O@C$ has C1s, O1s and Cu2p peaks, while $Cu(Im)_2$ derived Cu@N-C has C1s, N1s and Cu2p peaks (Figs. S8 and S14). After the carbonization of both MOF compounds, organic linkers transform themselves to form a carbonized structure consisting of a mixture of C-C sp^3, C=C sp^2, etheric C-O, C-OH, C=O and COOH peaks (Figure 6 and Table 1). It is seen that C-Cu peaks are located at 283.5 and 283.7 eV for $Cu/Cu_2O@C$ and Cu@N-C, respectively [37]. Apart from the $Cu/Cu_2O@C$, Cu@N-C possesses pyrrolic N- and pyridinic N- peaks because of the presence of N atoms in imidazole compound (Figure S13, Table 1). However, $Cu/Cu_2O@C$ also has Cu_2O peaks, as seen in the XRD spectrum (Figure 4).

Table 1. Binding energies and relative intensities of the catalysts

	Cu/Cu₂O@C		Cu@N-C	
	Binding Energy (eV)	**Atomic (%)**	**Binding Energy (eV)**	**Atomic (%)**
sp^2 C=C	284.0	14.7	284.2	13.1
sp^3 C-C	284.4	24.3	-	-
C-O-C	285.9	18.0	285.8	16.7
C-OH	284.9	24.4	284.8	28.5
C=O	-	-	287.4	14.0
HO-C=O	288.3	5.6	289.1	3.6
C-Cu	283.5	8.2	283.7	24.2
Pyrrolic N	-	-	400.1	11.2
Pyridinic N	-	-	398.2	88.9

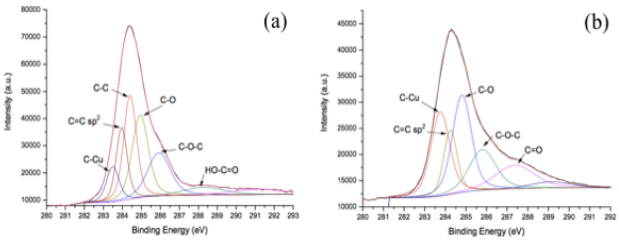

Figure 6. XPS data of (a) $Cu/Cu_2O@C$ and (b) Cu@N-C

For an enhanced catalytic reaction, the specific surface area and the pore size of the catalyst have significant functions. Using catalysts with high specific surface areas and wide pores are extremely important. Catalysts with high specific surface areas would get into contact with more reactants.

The MOF's synthesized after the hydrothermal synthesis were thermolized to obtain the catalysts. $Cu/Cu_2O@C$ catalyst was obtained after the thermolysis of $Cu_3(btc)_2$ and Cu@N-C catalyst was obtained after the thermolysis of $Cu(Im)_2$. According to the characterization results, the specific surface area of $Cu/Cu_2O@C$ was measured as 177 m^2/g. On the other hand, Cu@N-C's specific surface area was measured as 110 m^2/g. These results are consistent with the SEM images were denser and agglomerated particles were obtained after the thermolysis of $Cu(Im)_2$. These results point out that $Cu/Cu_2O@C$ is potentially a better catalyst for its higher specific surface area, where catalytic performances will be discussed in the following sections.

Both $Cu/Cu_2O@C$ and Cu@N-C showed a hysteresis loop in their adsorption/desorption curves which indicates that the catalysts are mesoporous (Figure S15 and S16). When the pore volumes of both samples were compared, it was seen that $Cu/Cu_2O@C$ has a larger pore volume value of 0.48 cm^3/g. However, the pore volume of Cu@N-C was only 0.12 cm^3/g due to agglomeration of the particles.

Figure 7 shows the BJH pore size distribution curves of the catalysts. Actually, both of the samples have similar pore sizes (dp($Cu/Cu_2O@C$) = 2.9 nm, dp(Cu@N-C) = 2.8 nm). However, the effect of thermolysis on Cu@N-C was more effective in terms of particle agglomeration and pore clogging. While $Cu/Cu_2O@C$ has a very sharp pore size peak, Cu@N-C's peak was very weak. Eventually, the agglomeration and pore-clogging caused a reduction in the surface area and pore volume. However, it should be noted that both of the particles have high specific surface areas and they should show improved catalytic performances.

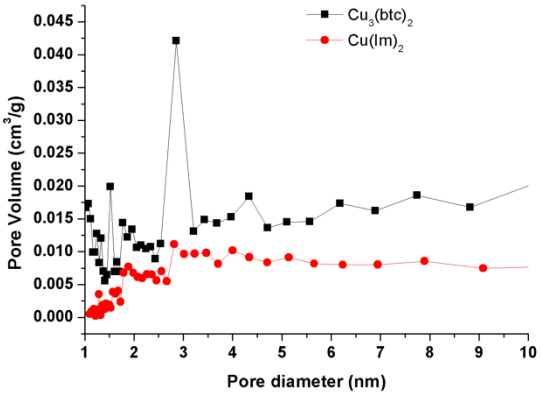

Figure 7. Pore size distribution curves calculated by the BJH method

Catalyst Reduction

The reaction mechanism for the reduction of an aromatic nitro compound is as follows (Scheme 1): It is firstly reduced to an aromatic-nitroso compound, followed by the formation of an intermediate aromatic hydroxylamine compound and finally to aromatic amine [38].

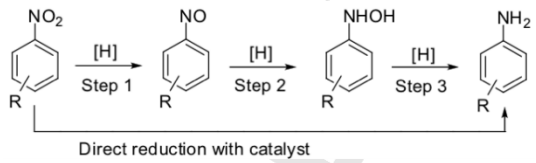

Scheme 1. Reduction steps of aromatic nitro compounds to aniline

The catalytic reduction reaction of 4-NA to PPD was carried out in the presence of as-synthesized $Cu_3(btc)_2$ derived $Cu/Cu_2O@C$ nanoparticles as the catalyst and $NaBH_4$ as co-catalyst. The reduction reaction was observed with UV-vis spectroscopy to monitor the disappearance of the 4-NA absorbance peak at 380 nm along with simultaneous appearance of two bands at 238 and 305 nm (Figure 8) suggesting that 4-NA is converted to PPD without any by-products. $NaBH_4$ is not itself able to reduce 4-NA in the absence of a catalyst [39]. On the other hand, the concentration of $NaBH_4$ is higher than the reactant 4-NA [$NaBH_4$]/[4-NA] = 40:1, the reduction reaction is considered as a pseudo-first order reaction.

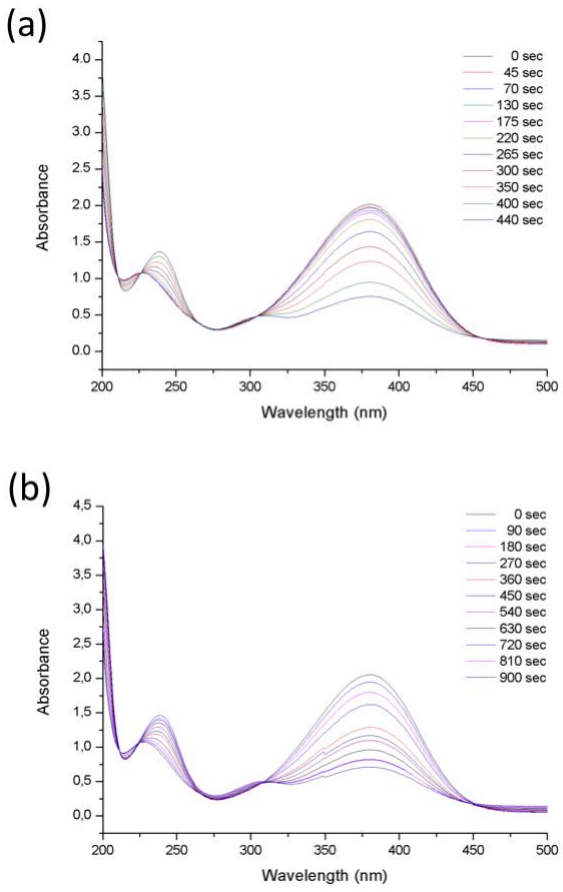

Figure 8. UV spectra of 4-nitroaniline to PPD in the presence of $Cu/Cu_2O@C$ (left) and Cu@N-C with 0.02 M $NaBH_4$ as co-catalyst

In the case of the reduction of 4-nitrobenzaldehyde, it was observed that the aldehyde group together with the nitro group was reduced in the presence of both catalysts. 4-nitrobenzaldehyde had the absorbance peak of 277 nm. When only the aldehyde group was reduced to form 4-aminobenzaldehyde, the absorbance peaks of 320 nm and 230 nm were expected to appear. However, we observed only one peak at 246 nm, which corresponds to 4-hydroxymethylaniline (Figure S23). Thus, the reduction of 4-nitrobenzaldehyde to 4-hydroxymethylaniline was successfully achieved.

The reduction of nitrobenzene resulted in aniline in the presence of $Cu/Cu_2O@C$ and Cu@N-C catalysts by using 0.1 M $NaBH_4$ as a co-catalyst. The catalytic reduction reaction was monitored by UV-vis spectroscopy and was confirmed by the disappearance of specific absorbance value of nitrobenzene at 268 nm. Subsequently, the formation of aniline was demonstrated by the appearance of the absorbance value of 230 nm belonging to aniline (Figure S24).

With the $Cu/Cu_2O@C$ catalyst, the conversion was found to be 100% for 4-NA whilst about 70% and 55% for 4-nitrobenzaldehyde and nitrobenzene, respectively (Figures S25-S27). This is most probably due to the substituent effect of the benzene ring. According to the conversion results electron-donating amino ($-NH_2$) group in 4-NA seems to be more easily reduced while electron-withdrawing group aldehyde (-CHO) in 4-nitrobenzaldehyde gives poor conversion yield.

The catalytic activity of the derived MOFs was determined by the k_{app} rate constant values of each catalyst (Table 2). The k_{app} values are determined by the Lambert-Beer law, the ratio of the concentrations initially (C_0) and any time (C_t) can be calculated by the ratio of the corresponding absorbance (A_t/A_0). Thus, the k_{app} values are directly calculated from the slope of the linear plots by using the formula for the first order kinetic reaction (Supplementary data, eq.1, Figure S22). Accordingly, it is clear that $Cu/Cu_2O@C$ is superior to the Cu@N-C when compared in terms of catalytic activity. From the results shown in Table 2, $Cu/Cu_2O@C$ tends to show about two-fold better activity than Cu@N-C. It is considered that the presence of Cu_2O in the $Cu/Cu_2O@C$ shows better catalytic activity than the Cu@N-C catalyst. The $Cu/Cu_2O@C$ catalyst obviously shows a better catalytical performance than Cu@N-C. $Cu/Cu_2O@C$ should perform due to its higher specific surface area and better pore structure. However, for most of the cases, the enhancement cannot be explained only by the surface area. The better catalytic activity of the $Cu/Cu_2O@C$ over Cu@N-C has also been attributed to the existence of facet-dependent Cu_2O nanoparticles in the $Cu/Cu_2O@C$ catalyst. It is reported that the sharp-faced rhombic octahedral and/or dodecahedral Cu_2O nanoparticles have shown a strong catalytic activity [40]. The reason for better catalytic activity of the $Cu_2O/Cu@C$ when compared with that of Cu@N-C can be attributed to rhombic octahedral morphology having sharp faces in our catalyst. Also, in the reduction of 4-nitrobenzaldehyde and 4-nitrobenzene, the Cu@N-C showed poor activity when compared with the $Cu/Cu_2O@C$ catalyst (Table S1).

Table 2. Rate constant k_{app} values of the $Cu/Cu_2O@C$ (left) and Cu@N-C catalysts in the reduction of 4-NA to PPD

Concentration of $NaBH_4$ [M]	**k_{app} for $Cu/Cu_2O@C$ (s^{-1})**	**k_{app} for Cu@N-C (s^{-1})**
0.02	0.0023	0.0013
0.03	0.0095	0.0008
0.04	0.0069	0.0018
0.05	0.0124	0.0032
0.10	0.0248	0.0100

For both catalysts, even though the Cu@N-C catalyst seems to have poor activity, when compared with other catalysts reported in the literature, it seems clear that it has a great strength over them. A comparison of some catalysts for the reduction of 4-NA to PPD has been presented in Table 3. Some of the rate constants were originally not given, but it has been reported that the reaction is completed in minutes. Hence, it is considered that the rate constants are lower than those of our catalysts.

Table 3. The reported catalysts for the reduction of 4-NA to PPD in the literature

Catalyst	k_{app}	Co-catalyst	Ref.
Iron oxide@Ni NP	-	$NaBH_4$	16
Fe_3O_4/SiO_2/Ag nanocubes	-	$NaBH_4$	20
Au NP	$7.575x10^{-2}$ min^{-1}	$NaBH_4$ (0.1M)	38
Ag NP@polyelectrolyte	0096 s^{-1}	$NaBH_4$	39
Au/pillar[5]arene	$8.34x10^{-3}$ s^{-1}	$NaBH_4$ (excess)	41
Pt@peptide hydrogels	-	$NaBH_4$	42
Cu/Cu_2O@C	0.0248 s^{-1}	$NaBH_4$ (0.1M)	Present work
Cu@N-C	0.01 s^{-1}	$NaBH_4$ (0.1M)	Present work

The conversion of the aromatic nitro compounds to aromatic amine derivatives are also illustrated for both Cu/Cu_2O@C and Cu@N-C. It is clear that the conversion was completed in the case of all concentrations of $NaBH_4$ except for 0.02 M of the Cu/Cu_2O@C catalyst (Figures S25 and S27). Contrarily, when Cu@N-C was used, only reduction reaction of 0.1 M $NaBH_4$ seemed to convert all 4-NA to PPD with 100% efficiency.

The reduction reactions of 4-nitroaniline, 4-nitrobenzaldehyde and nitrobenzene driven by the catalysts derived by the thermolysis of $Cu_3(btc)_2$ and $Cu(Im)_2$ compounds were studied. The composites obtained from copper-based metal organic frameworks have micro, meso, and macropores providing a better distribution of the composites on the surface. The obtained composite Cu/Cu_2O@C, which is derived from the $Cu_3(btc)_2$, demonstrated excellent activity whilst the composite Cu@N-C derived from the $Cu(Im)_2$ catalyst was found to have moderate activity, according to the rate constants, reduction times and conversion data. In conclusion, this study established that the tested copper-based composites show superior activity compared with the noble metals which are mostly used as reduction catalysts as stated in the literature. Additionally, Cu/Cu_2O@C and Cu@N-C composites are low-cost, eco-friendly and highly efficient for use in the reduction of aromatic nitro compounds to aromatic amines within seconds, offering potential for numerous applications.

Experimental Section

Materials and Instrumentation

Copper(II) nitrate hemi (pentahydrate) ($Cu(NO_3)_2.2.5H_2O$), copper(II) sulphate pentahydrate ($CuSO_4.5H_2O$), benzenetricarboxylic acid, imidazole, acetonitrile and ethanol were purchased from Sigma-Aldrich and 4-nitroaniline (4-NA), 4-nitrobenzaldehyde (4-NB), nitrobenzene (NB) and sodium bicarbonate ($NaHCO_3$) were purchased from Merck. All the chemicals were used without further purification.

For the XRD characterization, the analyses were performed with Cu Kα radiation wavelength of 1.5418 A° and step size 0.02 in the range of 2θ = 5 – 30° with a Bruker AXS-D8 diffractometer. Raman spectroscopy of carbon supports and catalysts were measured with a Renishaw Raman Spectrometer by a laser with an excitation line at 532 nm, a spectral range of 100 to 3200 cm^{-1}. To determine the morphological structure, scanning electron microscope FE-SEM Zeiss Leo Supra 35VP was utilized at 5 kV. Catalyst reduction was observed with a Varian Cary 5000 UV-vis-NIR Spectrometer. All XPS data were collected with a Thermo Scientific K-Alpha X-ray Photoelectron Spectrometer with a pass energy of 150 eV and dwell time of 5 ms. Thermogravimetric analysis was performed with a Shimadzu DTG-60H. The specific surface areas and pore characteristics of the catalysts were measured using a NOVA 2200e Surface Area and Pore Size Analyzer (Quantachrome Instruments Co.). The analyses were performed at 77 K (nitrogen gas boiling point). Samples were outgassed at 150 °C for 24 hours. BET surface areas were calculated using the data in the range of 0.05-0.3. The pore volume and pore size distributions were calculated using the adsorption branch of the isotherms by the Barrett–Joyner–Halenda (BJH) method.

Synthesis of $Cu_3(btc)_2$

The synthesis of $Cu_3(btc)_2$ was carried out according to the literature using a hydrothermal method [43]. 1.672 g of $Cu(NO_3)_2.2.5H_2O$ was dissolved in 24 mL of water while 0.440 g of benzenetricarboxylic acid (btc) was dissolved in 24 mL EtOH. These two solutions were mixed into a teflon-lined autoclave. The autoclave was kept at 120°C for 12h followed by cooling at ambient temperature. The suspension was poured into a falcon tube and centrifuged at least three times. After the precipitation process, a green solution and layered turquoise solid material were obtained.

Synthesis of $Cu(Im)_2$

The synthesis of copper(II) bisimidazolate was performed according to the method given in the literature [32]. In a 150 mL two-necked flask a solution of 1.36 g of imidazole (20 mmol) and 6.6 g of $NaHCO_3$ (78.56 mmol) in 50 mL of H_2O was heated in 80 °C with a water bath for 3 h. 2.5 g of $CuSO_4.5H_2O$ (10.1 mmol) in 12.5 mL of H_2O solution was added dropwise to the imidazole/$NaHCO_3$ solution while stirring. The formation of a violet precipitate was immediately observed. By leaving the mixture under reaction conditions, the violet compound was gradually transformed into blue colored compound of $Cu(Im)_2$. After 2h the blue compound was filtered off, washed with water and dried at 110°C in an oven overnight.

Thermolization of MOF Compounds

Both MOF compounds $Cu_3(btc)_2$ and $Cu(Im)_2$ have been thermolized according to the temperature obtained from TGA analysis. For this purpose, 0.5 mg of MOF compound was put into an alumina crucible and then placed into the tube furnace. Temperature ramp was set to 10°C per minute. After the thermolysis, the samples were allowed to cool at room temperature.

Catalytic Reduction Tests

The catalytic reduction tests were carried out in a standard quartz cuvette with 1 cm path length. Sodium borohydride ($NaBH_4$) was used as a co-catalyst during the reduction process. The reaction has been monitored with the formation of characteristic absorbance peaks of aromatic amines and the disappearance of aromatic nitro absorbance peaks via UV-vis spectrometer. A 0.20 mL of substrate solution with 2.5 mM dissolved in an appropriate solvent (water for 4-nitroaniline and acetonitrile for 4-nitrobenzaldehyde and nitrobenzene) was mixed with 0.2 mL of $NaBH_4$ solution with different concentrations. Subsequently, 80 μL of aqueous dispersion of the catalyst (10 mg/mL) was added, and solution was immediately subjected to UV-vis measurements.

Acknowledgements

The authors would like to thank Daniel Lee Calvey and Muhammad Faisal Jamil for proof-reading the article. The author Emre Biçer is also grateful to Prof. Dr. Ender Erdik for sharing her class notes on organometallics.

Keywords: Metal-Organic Frameworks, Catalyst, Aromatic Nitro Compounds, Reduction

[1] J.Y. Lee, J. Li, J. Jagiello, *J. Solid State Chem.* **2005**, 178, 2527-2532.
[2] J. Wei, Y. Hu, Y. Liang, B. Kong, J. Zhang, J. Song, Q. Bao, G.P. Simon, S.P. Jiang, and H. Wang, *Adv. Funct. Mater.* **2015**, 25, 5768-5777.
[3] Y. Gao, J. Wu, W. Zhang, Y. Tan, J. Gao, J. Zhao and B. Tang, *New J. Chem.* **2015**, 39, 94-97.
[4] L. Wang, Y. Han, X. Feng, J. Zhou, P. Qi, B. Wang, *Coor. Chem. Rev.* **2016**, 307, 361-381.
[5] K. Shen, X. Chen, J. Chen, Y. Li, *ACS Catal.* **2016**, 6, 5887-5903.
[6] N. Ahmad, H.A. Younus, A.H. Chughtai and F. Verpoort, *Chem. Soc. Rev.* **2015**, 44, 9-25.
[7] A.H. Chughtai, N. Ahmad, H.A. Younus, A. Lyapkov and F. Verpoort, *Chem. Soc. Rev.* **2015**, 44, 6804-6849.
[8] Y. Yusran, D. Xu, Q. Fang, D. Zhang, S. Qiu, *Microporous Mesoporous Mater.* **2017**, 241, 346-354.
[9] K.-Y. A. Lin, H.-A. Chang, R.-C. Chen, *Chemosphere* **2015**, 130, 667-672.
[10] X. Wang, X. Li, C. Ouyang, Z. Li, S. Dou, Z. Ma, L. Tao, J. Huo and S. Wang, *J. Mater. Chem. A* **2016**, 4, 9370-9374.
[11] Z. Wang, T. Yan, L. Shi, and D. Zhang, *ACS Appl. Mater. Interfaces* **2017**, 9, 15068-15078.
[12] L. Yan, Y. Liu, K. Zha, H. Li, L. Shi, and D. Zhang, *ACS Appl. Mater. Interfaces* **2017**, 9, 2581-2593.
[13] L. Zhang, L. Shi, L. Huang, J. Zhang, R. Gao, and D. Zhang, *ACS Catal.* **2014**, 4, 1753-1763.
[14] C. Yu, B. Liu, and L. Hu, *J. Org. Chem*. **2001**, 66, 919-924.
[15] A.K. Shil and P. Das, *Green Chem.* **2013**, 15, 3421-3428.
[16] P.S. Rathore, R. Patidar, T. Shripathi and S. Thakore, *Catal. Sci. Technol.* **2015**, 5, 286-295.
[17] W. Wu, G. Liu, Q. Xie, S. Liang, H. Zheng, R. Yuan, W. Su and L. Wu, *Green Chem.* **2012**, 14, 1705-1709.
[18] W. Wu, G. Liu, S. Liang, Y. Chen, L. Shen, H. Zheng, R. Yuan, Y. Hou, L. Wu, *J. Catal.* **2012**, 290, 13-17.
[19] W. Wu, S. Liang, Y. Chen, L. Shen, H. Zheng, L. Wu, *Catal. Commun.* **2012**, 17, 39-42.
[20] M. Abbas, S.R. Torati and C.G. Kim, *Nanoscale* **2015**, 7, 12192-12204.
[21] Z. Hasan, D.-W. Cho, C.-M. Chon, K. Yoon, H. Song, *Chem. Eng. J.* **2016**, 298, 183-190.
[22] X.-X. Guo, D.-W. Gu, Z. Wu, and W. Zhang, *Chem. Rev.* **2015**, 115, 1622-1651.
[23] M.B. Gawande, A. Goswami, F.-X. Felpin, T. Asefa, X. Huang, R. Silva, X. Zou, R. Zboril and R.S. Varma, *Chem. Rev.* **2016**, 116, 3722-3811.
[24] S.S.-Y. Chui, S.M.-F. Lo, J.P.H. Charmant, A.G. Orpen, I.D. Williams, *Science* **1999**, 283, 1148-1150.
[25] L. Alaerts, E. Séguin, H. Poelman, F. Thibault-Starzyk, P.A. Jacobs, D.E. De Vos, *Chem. – Eur. J.* **2006**, 12, 7353-7363.
[26] M. Wang, M.H. Xie, C.D. Wu, and Y. Wang, *Chem. Commun.* **2009**, 17, 2396-2398.
[27] L.X. Shi, and C.D. Wu, *Chem. Commun*. **2011**, 47, 2928-2930.
[28] I. Luz, F.X. Llabrés i Xamena, A. Corma, *J. Catal.* 2010, 276, 134-140.
[29] D. Shi, Y. Ren, H. Jiang, B. Cai, and J. Lu, *Inorg. Chem.* **2012**, 51, 6498-6506.
[30] A. Schejn, A. Aboulaich, L. Balan, V. Falk, J. Lalevée, G. Medjahdi, L. Aranda, K. Mozeta and R. Schneider, *Catal. Sci. Technol*. **2015**, 5, 1829-1836.
[31] L.H. Wee, N. Janssens, S.R. Bajpe, C.E.A. Kirschhock, J.A. Martens, *Catalysis Today* **2011**, 171, 275-280.
[32] N. Masciocchi, S. Bruni, E. Cariati, F. Cariati, S. Galli, and A. Sironi, *Inorg. Chem.* **2001**, 40, 5897-5905.

[33] I. Luz, A. Corma and F.X. Llabrés i Xamena, *Catal. Sci. Technol.* **2014**, 4, 1829-1836.
[34] J.-Y. Ye and C.-J. Liu, *Chem. Commun.* **2011**, 47, 2167-2169.
[35] B. Panella and M. Hirscher, *Phys. Chem. Chem. Phys.* **2008**, 10, 2910-2917.
[36] M. Yin, C.-K. Wu, Y. Lou, C. Burda, J.T. Koberstein, Y. Zhu, and S. O'Brien, *J. Am. Chem. Soc.* **2005**, 127, 9506-9511.
[37] P.A. Chen, *Thin Solid Films* **1991**, 204, 413-416.
[38] C.-Y. Chiu, P.-J. Chung, K.-U. Lao, C.-W. Liao, M.H. Huang, *J. Phys. Chem. C* **2012**, 116, 23757-23763.
[39] P. Viswanathan, R. Ramaraj, *J. Mol. Catal. A: Chem*. **2016**, 424, 128-134.
[40] M.B. Gawande, A. Goswami, F.-X. Felpin, T. Asefa, X. Huang, R. Silva, X. Zou, R. Zboril, R.S. Varma, *Chem. Rev.* **2016**, 116, 3722-3811.
[41] Y. Yao, M. Xue, X. Chi, Y. Ma, J. He, Z. Abliz and F. Huang, *Chem. Commun*. **2012**, 48, 6505-6507.
[42] I. Maity, D.B. Rasale and A.K. Das, *Soft Matter* **2012**, 8, 5301-5308.
[43] K.-S. Lin, A.K. Adhikari, C.-N. Ku, C.-L. Chiang, H. Kuo, *Int. J. Hydrogen Energy* **2012**, 37, 13865-13871.

10.1002/ejic.201701320

WILEY-VCH

Entry for the Table of Contents

Layout 1:

FULL PAPER

Copper-based MOF-derived catalysts for the reduction of aromatic nitro compounds have been studied in the current article.

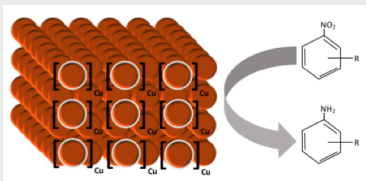

Key Topic*: Copper-based MOF, MOF-derived catalyst, aromatic nitro reduction

Özlem Karahan, Emre Biçer, Adnan Taşdemir , Alp Yürüm, Selmiye Alkan Gürsel,*

Page No. – Page No.

Title
Development of Efficient Copper-Based MOF-Derived Catalysts for the Reduction of Aromatic Nitro Compounds

*one or two words that highlight the emphasis of the paper or the field of the study